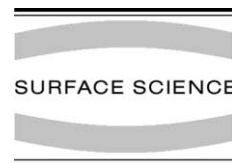




ELSEVIER

Surface Science 515 (2002) 553–566



www.elsevier.com/locate/susc

Phosphine adsorption and the production of phosphide phases on Cu(001)

L.V. Goncharova, S.K. Clowes¹, R.R. Fogg², A.V. Ermakov, B.J. Hinch^{*}

Department of Chemistry and Chemical Biology, Wright-Riemen Laboratories, Laboratory for Surface Modification, Rutgers University, 610 Taylor Road, Piscataway, NJ 08854-8087, USA

Received 15 February 2002; accepted for publication 10 June 2002

Abstract

The adsorption and thermal decomposition of PH_3 on a Cu(001) surface has been investigated by means of high-resolution helium atom scattering, Auger electron spectroscopy and temperature programmed desorption. Phosphine adsorption at $T_x < 160$ K produces a molecular overlayer structure with short-range order. Annealing of the low-temperature structure results in decomposition of the adsorbed PH_3 , and desorption of hydrogen between $T_x = 250$ K and $T_x = 320$ K. Molecular phosphine was not seen to desorb. Phosphine deposition at room temperature or above produces well-ordered copper–phosphorus phases exhibiting either $c(6 \times 8)$ or $c(6 \times 6)$ diffraction patterns, depending upon the deposition conditions. Auger electron spectra indicate that these ordered phases contain approximately $1/3$ ML or more of phosphorus. Possible atomic models for the overlayer structures are discussed.

© 2002 Elsevier Science B.V. All rights reserved.

Keywords: Atom–solid scattering and diffraction – inelastic; Surface structure, morphology, roughness, and topography; Sticking; Copper; Phosphine; Single crystal surfaces

1. Introduction

For many years, trivalent phosphorus-containing molecules (such as phosphine or its alkyl derivatives) have been used for P doping of semiconductor materials [1–3]. Several studies have also shown that small amounts of phosphine

strongly influence the growth kinetics of silicon [4,5] by saturation of Si dangling bonds [6]. In addition, simple phosphine molecules such as alkyl and halo phosphines are often the ligands of choice in metalorganic chemical vapor deposition (MOCVD) [7]. Unlike alkyl radicals (which are possible alternative ligands in MOCVD precursors) phosphine ligands are molecular species; and the oxidation of metal centers is limited in the phosphine based MOCVD precursors. Despite their importance, the chemistry of phosphine molecules on transition metal surfaces has only recently received much attention. Essentially very little is known about the weak metal–phosphorus interactions at surfaces.

^{*} Corresponding author. Tel.: +1-732-445-0663; fax: +1-732-445-5312.

E-mail address: jhinch@rutchem.rutgers.edu (B.J. Hinch).

¹ Present address: Experimental Solid State Group, Imperial College, London SW7 2BZ, UK.

² Present address: Department of Physics, Cornell University, Ithaca, NY 14850, USA.

Several comparative studies [8–10] have concluded that PH_3 is less stable than PF_3 on transition metal surfaces. On $\text{Ag}(1\ 1\ 1)$ [10] PH_3 adsorbs molecularly for all coverages at 100 K. On other metal surfaces, such as $\text{Ni}(0\ 0\ 1)$ [11], $\text{Rh}(0\ 0\ 1)$ [12], and $\text{Pt}(1\ 1\ 1)$ [13], phosphines adsorb dissociatively at low coverages, followed by physisorption of molecular phosphine species at higher exposures. Desorption of molecular phosphine was observed for $\text{Ag}(1\ 1\ 1)$ [10], $\text{Rh}(0\ 0\ 1)$ [14] and polycrystalline iron [12]. In contrast, for PH_3 adsorption on $\text{Pt}(1\ 1\ 1)$ [13] and $\text{Ni}(0\ 0\ 1)$ [15] no phosphorus-containing species leave the surface, only hydrogen desorption was observed. The complex decomposition path of $\text{PH}_3 \rightarrow \text{PH}_x \rightarrow \text{P}$ was explicitly shown for the $\text{Ru}(0\ 0\ 0\ 1)$ [9] surface at ~ 190 K. The only published reports of phosphine adsorption on copper is a study of PH_3 adsorption on 1–10 ML thick Cu films on $\text{Ru}(0\ 0\ 0\ 1)$ [8]. It was shown [8] that PH_3 adsorbs primarily in the molecular form at 80 K. This study also demonstrated that phosphine has a relatively large electronic dissociative cross section (of the order of 10^{-16} cm²). This observation goes part way to explaining why ordered molecular phosphine surface structures have, thus far, not been reported.

On the $\text{Cu}(1\ 1\ 1)$ surface [16] it was shown that (more stable) PF_3 molecules are bonded atop with its threefold axis oriented along the surface normal. Jackson et al. [17] found that molecular fragments, such as PF_2 , P and P_2F_x , can also occupy bridge (PF_2) and fcc hollow (P and P_2F_x) sites. Similar adsorption sites could be expected for PH_3 and its fragments.

Coadsorption of phosphine with other molecular species (CO , D_2 , H_2 and O_2) has also been investigated for the $\text{Pt}(1\ 1\ 1)$ [13], $\text{Ni}(0\ 0\ 1)$ [15], and $\text{Rh}(0\ 0\ 1)$ [14] surfaces. Preadsorbed PH_3 was found to reduce D_2 , H_2 and CO saturation levels on $\text{Pt}(1\ 1\ 1)$ [13], influence CO and H_2 adsorption rates and saturation coverages on $\text{Ni}(0\ 0\ 1)$ [15], and reduce hydrogen adsorption levels on $\text{Rh}(0\ 0\ 1)$ [14]. In contrast, postdosed PH_3 can displace 60–65% of H (D) or O from $\text{Rh}(0\ 0\ 1)$ [14]. Unfortunately, the literature does not contain reports on coadsorbate-induced changes in phosphine sticking coefficients.

Helium atom scattering (HAS) is extremely sensitive to the lateral distributions of adsorbates on a surface and is ideal for the study of systems that are highly susceptible to electron beam damage. In this paper we use primarily HAS, as well as Auger electron spectroscopy (AES) and temperature programmed desorption (TPD) to investigate the PH_3 on $\text{Cu}(0\ 0\ 1)$ adsorption system. The experimental section below details unusual aspects of our measurements. The results of low and high-temperature phosphine adsorption studies are presented. We then discuss essential features of the observed copper–phosphorus structures, and models for $c(6 \times 8)$ and $c(6 \times 6)$ phases are proposed.

2. Experiment

The apparatus used in these experiments has been described in detail elsewhere [18]. The equipment is centered around a high-resolution HAS instrument. Phosphine adsorption and desorption was monitored in specularly reflected helium atom intensity measurements, at different substrate temperatures. The specular condition for the sample uses equal incident and emerging angles, $\theta_i = \theta_f = 49.5^\circ$. In addition, TPD spectra, for $m = 2$ (H_2^+) and $m = 34$ (PH_3^+), and helium reflectivities were recorded simultaneously at a sample temperature, T_x , heating rate of 2 K/s. For these measurements a quadrupole mass spectrometer (UTI QMS) is used in direct line of sight of the sample, but at an angle of 55° with respect to the surface normal. The ion extraction region (cage) has a diameter of ~ 8 mm, and is approximately 5 cm from the sample surface. Additional skimmers and collimators are placed between the ionization region and the sample.

TPD scans can also be made (without monitoring He specular reflectivity) with a reduced angle between the QMS and the surface normal. However, angles below $\sim 25^\circ$ cannot be obtained, due to other obstructions in the system. The important implication of this fact is the lack of sensitivity to hydrogen desorption from clean Cu surfaces, which are reportedly highly directional around the surface normal in the range 370–800 K

[19]. In fact, we see only a minority H_2 species desorbing from defects on the Cu(001) surface, at $T_x \sim 340$ K. For this case, it is indeed the He reflectivity that is most sensitive to H_2 desorption which we observe at 300 K. At this point in time, we have no reason to suppose that any other species desorb so directionally from the surfaces we have investigated here and, we believe that all desorption processes do show up in He reflectivities and/or TPD scans.

High-resolution elastic helium diffraction scans (taken both in-plane $[1\bar{1}0]$ and out-of-plane scattering directions) have been used to determine the overlayer periodicities. Time-of-flight measurements were used to determine the incident He beam energies. This method of energy analysis was also utilized in “drift” spectra, in which the helium beam energy changes as the He nozzle temperature is ramped from 60 to 330 K.

The sample was cleaned in vacuum with repeated cycles of neon ion sputtering and annealing to 700 K, and with final anneals to 900 K. The surface temperature was controlled using a Chromel–Alumel (K-type) thermocouple, which was attached directly to the side of the sample. We estimate an accuracy of ± 5 K in the measurement of the absolute surface temperature using this method and a reproducibility to better than 1 K.

Phosphine (99.99% purity, Matheson) exposures were performed by backfilling the chamber to a pressure of $<10^{-8}$ Torr through a leak valve. The stated exposures (measured in Langmuir, $1\text{ L} = 10^{-6}$ Torr s) were calculated using an uncalibrated ion gauge. AES was performed using a double pass cylindrical mirror analyzer.

3. Results

The inert helium atom reflectivity measurements prove to be valuable in establishing temperature/exposure regimes for PH_3 exposure of the Cu(001) surface. Different temperature and exposure ranges can be identified within the uptake curves of Fig. 1, indicating the possible onset and completion of distinct processes. The helium atom reflectivity from highly reflective metallic substrates is closely related to the number density and

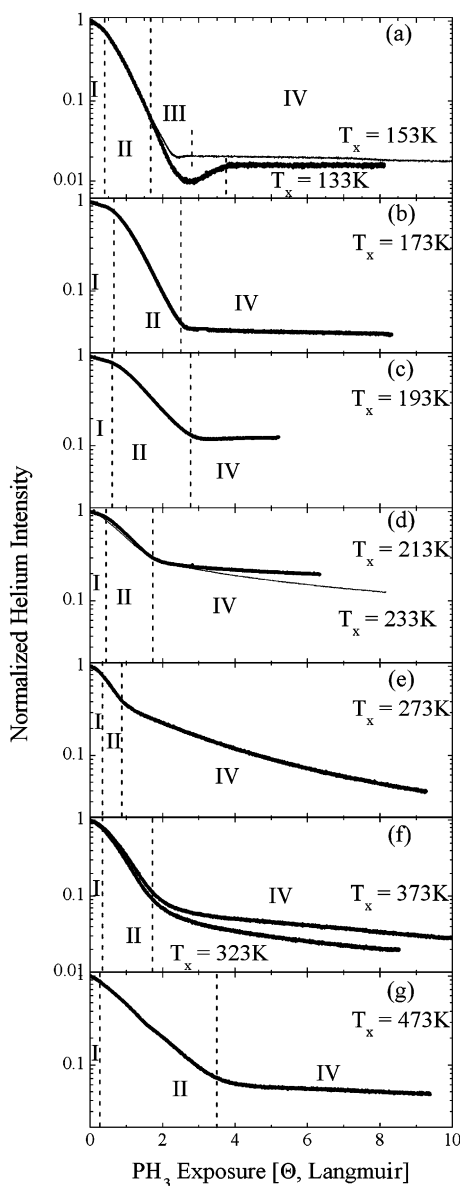


Fig. 1. Specularly scattered helium signal during PH_3 exposure for different fixed sample temperatures (a)–(g), all at $\theta_i = 49.5^\circ$ and $E_i = 27$ meV. Different adsorption behavior regions are designated by capital roman numbers I through IV.

effective cross sections of adsorbed species [20]. The cross sections of adsorbates for the helium atoms usually varies considerably depending upon the location and the nature of the adsorbed species. For PH_3 exposures one might anticipate

adsorbed molecular PH_3 , molecular fragments (PH_x , $x = 1, 2$), atomic H, and/or even atomic phosphorus dependent on the substrate temperature. At the highest surface temperatures investigated P can also diffuse into the substrate forming bulk copper phosphides [21,22]. Briefly, a change in gradient or shape of the curves in Fig. 1 implies either a change in sticking coefficients or a change in the character of an adsorbed species, all at a specific surface temperature.

Fig. 1 is subdivided into panels (a) through (g) in an effort to highlight the changes in the forms of the curves as the temperature increases. For clarity we identify regions I–IV in the phosphine uptake curves. Region I corresponds to a short initial region with approximately linear reflectivity decrease and with a “small cross section”. Region I is longest at 173 K, extending to exposures of ~ 0.7 L, at other temperatures it typically runs from 0 to 0.3–0.5 L. Region II refers to a section of the curve that shows near logarithmic reflectivity decreases and with a higher cross section. Region II runs from ~ 0.25 to ~ 2 L at lower temperatures (133–153 K), from ~ 0.5 to ~ 2.5 L at 173–193 K, then decreases in range and is shortest at 273 K, and increases in range again up to ~ 3.5 L at 473 K. Region III corresponds to an intensity recovery with exposure and is prominent in the 133 and 153 K curves only. Region IV corresponds to a generally slower intensity variation that can have either zero or negative gradient. The onset of region IV is locally latest at 193 K, at ~ 3 L. At this, and lower temperatures, the reflected He signal has close to zero gradient. Above 193 K the gradient of region IV is negative and its magnitude increases with increasing temperature up until ~ 273 K. At 273 K, also, the minimum exposure (1 L) is used to achieve the onset of region IV. Above 273 K, the gradient reduces again and approaches zero at 473 K.

At the lowest temperature of these measurements, 133 K, and at exposures above ~ 4 L, only zeroth and first order diffraction spots are observed along the high symmetry $\langle 1\bar{1}0 \rangle$ direction, characteristic of a lattice gas adsorption. Yet, short-range ordering is apparent in the out-of-plane diffuse helium diffraction intensities, as shown in the intensity map in the inset of Fig. 2.

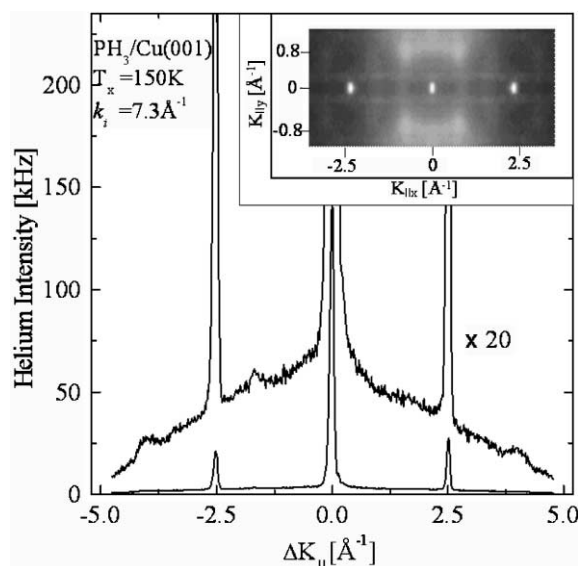


Fig. 2. A total He scattering intensity angular distribution, transformed to parallel momentum transfers, K_{\parallel} , along the $[1\bar{1}0]$ direction for PH_3 adsorbed on $\text{Cu}(001)$ at $T_x = 150$ K. The incident He energy, E_i , was 27 meV. The insert shows the helium diffraction pattern in two dimensions, around the central scattering plane. It reveals intensity maxima, i.e. weak $(\pm 1/3, \pm 1/3)$ diffraction peaks, corresponding to a poorly ordered $c(\sqrt{2} \times 3\sqrt{2})R45^\circ/\text{Cu}(001)$ overlayer structure.

The diffuse intensity is maximal at the $(\pm 1/3, \pm 1/3)$ diffraction positions.

The variation of the specular helium reflectivity in a TPD experiment from the low-temperature $\text{PH}_3/\text{Cu}(001)$ structure (as used in Fig. 2) is presented in Fig. 3. The dashed line represents the differential of the helium reflectivity curve. It emphasizes the reflected helium intensity increases seen at $T_x \cong 230$ K (α), 270 K (β) and 420 K (γ). Through this, and similar scans, molecular phosphine desorption is not seen. The only desorbing species observed are hydrogen molecules around 270 K, as illustrated in Fig. 3. At the end of this specific temperature ramp a new $c(6 \times 8)$ phase is present. This phase is discussed further below.

Even for the smallest PH_3 exposures at 273 K and above the helium atom diffraction maps indicate short-range ordering. In each case the extent of ordering can be improved dramatically by post annealing above 420 K. Fig. 4 shows in-plane intensity scans taken through ordered $c(6 \times 8)$ and

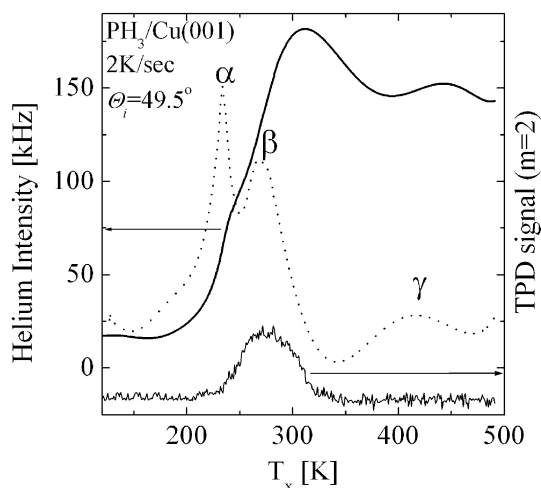


Fig. 3. Specularly reflected helium intensities (solid curve and left scale) and mass two hydrogen desorption signal (lower curve and right scale) during a surface temperature ramp following phosphine saturation at $T_x = 133$ K. Debye–Waller corrections to the helium intensities have not been applied. The dashed curve (arbitrary units on a linear scale) shows the temperature differential of the reflected helium intensity.

$c(6 \times 6)$ phases. The former phase could be prepared by exposure to PH_3 at $T_x < 273$ K and annealing to 523 K or by exposure at $T_x > 473$ K alone. The pure $c(6 \times 6)$ phase can be produced only by PH_3 exposures in the surface temperature range $T_x = 273$ – 373 K. Deposition of phosphine at $T_x \geq 473$ K or annealing of the $c(6 \times 6)$ reconstructed surface for a long period of time ($T_{\text{anneal}} < 473$ K, > 1 h) leads to a $c(6 \times 8)$ structure. On the other hand additional phosphine adsorption at $T_x > 323$ K on the $c(6 \times 8)$ structure can result in the reformation of the higher phosphorous coverage $c(6 \times 6)$ structure.

Two-dimensional (2-D) He intensity diffraction maps of the $c(6 \times 8)$ and $c(6 \times 6)$ phases are shown in Fig. 5(a) and (b), respectively. In the displayed $c(6 \times 6)$ phase diffraction map, (a) the majority of the back-reflected intensity is contained in the specular, the four $(\pm 1/6, \pm 1/6)$, the two $(\pm 1/3, 0)$ and the two $(0, \pm 1/3)$ peaks, i.e. close to the specular direction. The other weaker diffraction peaks also display an intensity maximum at a wider angle. This data, and other data taken at other He incident energies, are indicative of two rainbow angles in the $c(6 \times 6)$ and $c(6 \times 8)$ super-

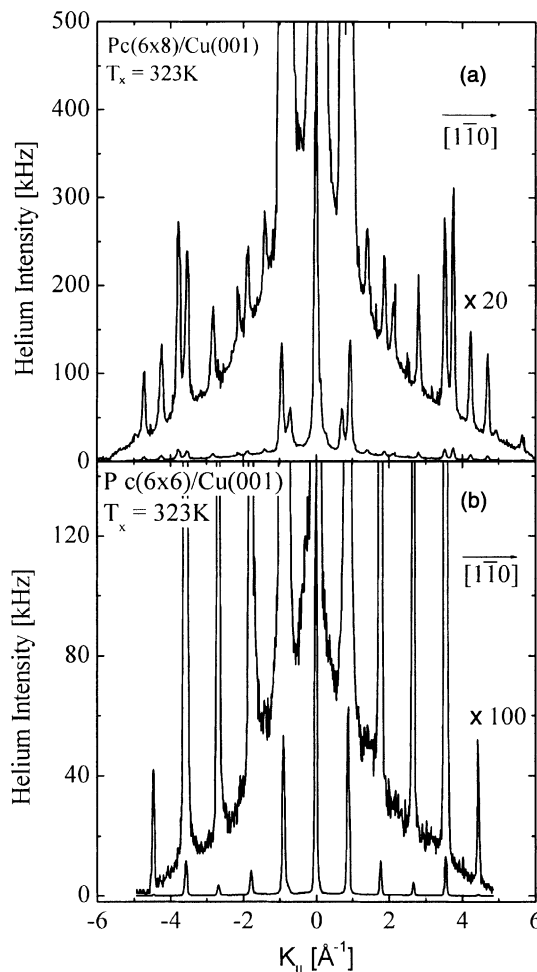


Fig. 4. He atom intensity angular distribution scans, $E_i = 27$ meV. (a) The $Pc(6 \times 8)$ overlayer produced by phosphine saturation at $T_x = 273$ K followed by short annealing to $T_x = 520$ K (~ 2 min); (b) the residual phosphorus $c(6 \times 8)/\text{Cu}(001)$ structure obtained after PH_3 saturation at $T_x = 133$ K, and annealing to $T_x = 520$ K for 2 min.

structures. The narrower angle is $\sim 4 \pm 1^\circ$, and the wider angle (more distant from the surface normal) is at $\sim 21 \pm 1^\circ$.

Another simple comparative analysis of the helium diffraction peak intensities provides additional information on the $c(6 \times 6)$ structure. In a 2-D helium diffraction pattern, as presented in Fig. 5(a), the intensities of the $(\pm 1/3, 0)$ peaks (“C”) differ from that of the $(0, \pm 1/3)$ peaks (“D”) by as much as 60–80%. Also the intensities of the four

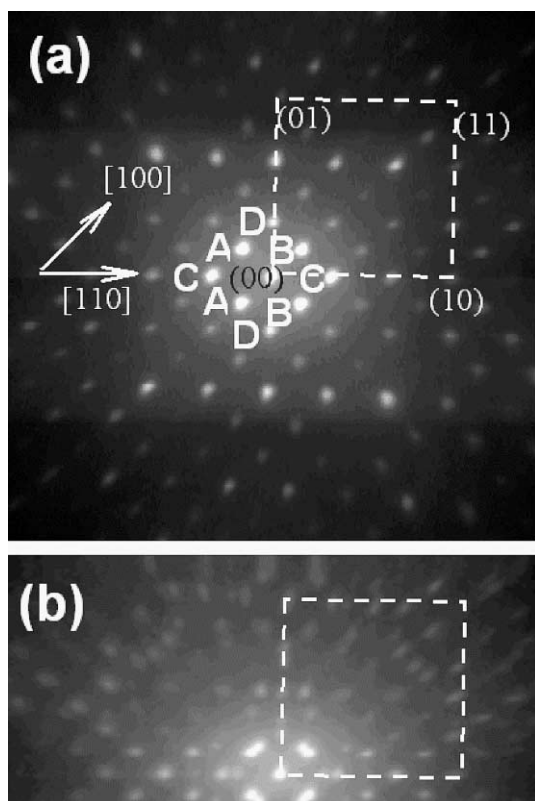


Fig. 5. Helium atom diffraction patterns constructed from angular distribution scans, similar to those of Fig. 4, with an incident beam energy of 63 meV and a sample temperature of 323 K. A dashed line indicates the substrate 1×1 unit cell. (a) The P $c(6 \times 6)$ reconstruction on Cu(001), produced by a saturating phosphine exposure at $T_x = 323$ K and a 2 min anneal to $T_x = 520$ K. (b) The P $c(6 \times 8)$ reconstruction, occurring after a saturating phosphine exposure at $T_x = 140$ K, and annealing to $T_x = 520$ K for 2 min.

$(\pm 1/6, \pm 1/6)$ peaks (designated by “A” and “B”) are very similar, but strictly do not show a fourfold symmetry.

In the $c(6 \times 8)$ diffraction pattern, both $(\pm 1/6, \pm 1/8)$ and $(\pm 1/8, \pm 1/6)$ diffraction spots are observed as there are necessarily two possible orientations, i.e. the $c(6 \times 8)$ and $c(8 \times 6)$ domains, on the Cu(001) surface. The intensities of the $(\pm 1/6, \pm 1/8)$ and the $(\pm 1/8, \pm 1/6)$ peaks, however, are not equivalent. Apparently this Cu(001) supported more of the $c(6 \times 8)$ domains, (as $I_{(\pm 1/6, \pm 1/8)} > I_{(\pm 1/8, \pm 1/6)}$). Also, the intensities of the four $(\pm 1/6, \pm 1/8)$ peaks (Fig. 5(b)) are essentially

identical, showing symmetry with two perpendicular mirror planes.

Fig. 6 illustrates typical Auger electron spectra sections taken after PH_3 exposures at 140 K (a), and 323 K (b). The low-temperature phase shows an unresolved triplet feature between 113 and 122 eV, attributable to P atoms. After annealing of the structure, a doublet remains between 119 and 122 eV. We take the P $L_{2,3}VV$ line shape, as measured at 323 K, as evidence of strong chemical bonding between topmost P atoms and substrate Cu atoms. A near identical P line shape was observed during Cu deposition on GaP [23,24]. In the GaP experiments, the P $L_{2,3}VV$ line shape changed from a single line (for GaP) to a doublet as a copper film thickness increased. The doublet was attributed to P that had diffused into the Cu adlayer.

For simplicity, as all AES scans were taken with identical resolution, we can deduce some relative P coverages by use of a normalized Auger feature ratio, AR. The latter was determined as the ratio of an integrated area under the P $L_{2,3}VV$ (112–120 eV) peak to a Cu M_{VV} (105 eV) peak height. These

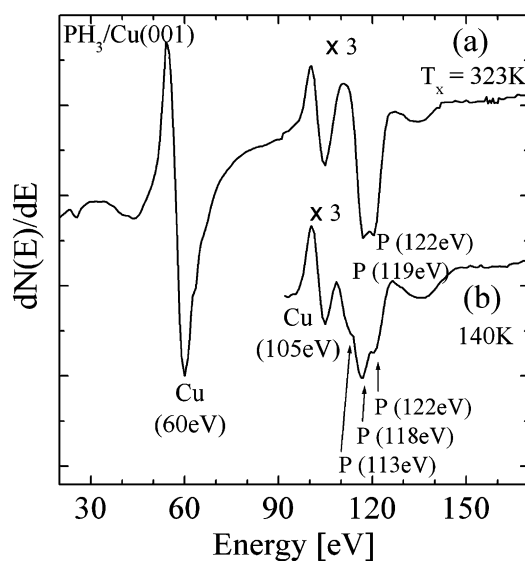


Fig. 6. Sections of Auger electron spectra, showing Cu ($M_{2,3}VV$) and P ($L_{2,3}VV$) transitions, (a) for a low-temperature PH_3 $c(\sqrt{2} \times 3\sqrt{2})R45^\circ/\text{Cu}(001)$ overlayer phase at 140 K and (b) for a P $c(6 \times 8)$ structure obtained by annealing the surface of (a) to $T_x > 450$ K. Both spectra have been normalized to give the same, constant Cu (60 eV) feature peak height.

Table 1
Auger feature ratio, AR, following saturation PX_3 exposures on Cu(001)

AES ratios, $P_{L_{2,3VV}}(119 \text{ eV})/$ $Cu_{M_{VV}}(105 \text{ eV})$	$AR_{LT \text{ phase}}$	$AR_{c(6 \times 8) \text{ phase}}$	$AR_{c(6 \times 6) \text{ phase}}$
PH_3	1.02 ± 0.03	1.28 ± 0.03	1.72 ± 0.03
PF_3	0.80 ± 0.04	0.97 ± 0.02	–

AR ratios for a low-temperature (140 K) saturation structure and a $c(6 \times 8)$ phase, obtained after annealing of the low-temperature phase to $T_x > 523$ K, are presented in Table 1.

Incidentally, we have found that the $c(6 \times 8)$ structure, discussed here, can be produced also by annealing PF_3 saturated ($T_x < 173$ K) Cu(001) surfaces to $T_x > 473$ K. For these annealed PF_3 surfaces, the Auger line shapes look identical to that for the annealed PH_3 surfaces and equivalent AR ratios are also presented in the Table 1. For either adsorbed phosphine, PH_3 or PF_3 , the AR ratio increases with annealing. Therefore, we make no attempt to compare the AR factors when the two different Auger line shapes are present. Instead, we shall make use only of the AR ratio comparisons for systems with identical line shapes. The highest P Auger signals are seen for the P $c(6 \times 6)$ phase, $AR_{6 \times 6} = 1.72 \pm 0.03$ observed after PH_3 exposures above 273 K.

Helium atom specularly backscattered intensities were also measured as a function of the incident beam energy. In these measurements, also called “drift spectra”, the specular intensity variations can be dominated by interference between different levels (or terraces) of the surface. The simple Bragg relationship describes this effect: $n = 2d \cos \Theta_i / \lambda$, where λ is the helium wavelength, and d is an interlayer separation. When n has an integral value constructive interference occurs and an intensity maximum is observed. And for n half-integral destructive interference gives rise to intensity minima. However, our drift spectra, show many minima features, common to highly corrugated surfaces. A pronounced bound-state resonance structure is implied which would be very difficult to interpret precisely given the large number of open diffraction channels. Drift spectra for the P $c(6 \times 6)/Cu(001)$ are presented in Fig. 7.

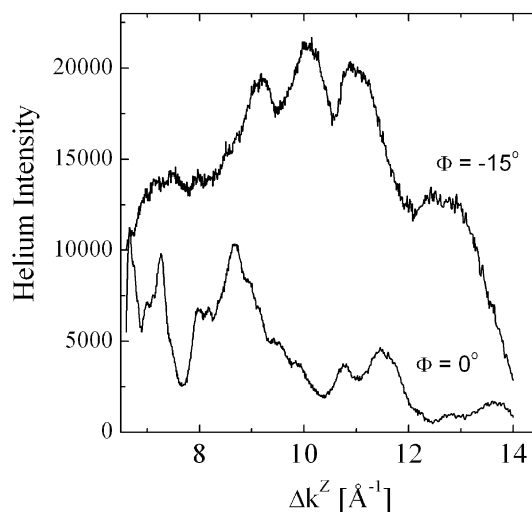


Fig. 7. Variations of experimental helium specular reflectivity ($\Theta_i = 49.5^\circ$) as a function of perpendicular momentum transfer, Δk^Z , for the P $c(6 \times 6)$ structure at $T_x = 323$ K. Scans are shown for two different scattering azimuths, $\Phi = 0^\circ$ and $\Phi = -15^\circ$ with respect to the $[110]$ scattering azimuth. A normalization (Jacobian) factor has been applied; a linear nozzle temperature ramp was used, and the data plotted as a function of Δk^Z .

Virtually no features are observed in common to both curves in Fig. 7; features are not reproduced from one scattering azimuth to another. Unfortunately, we were not able to extract meaningful superstructure height information from these drift measurements.

4. Discussion

4.1. Molecular PH_3 adsorption, thermal stability, and decomposition processes

In previous studies a region in uptake curves, such as region I, has usually been attributed to molecular adsorption at defect sites, e.g. step edges. After saturation of these sites, the adsorption is then seen on defect free terrace sites (region II). Region III has typically been associated with the onset of ordering and formation of ordered phases. After the end of region III, slow intensity variations may be anticipated, as the sticking coefficients can be dramatically decreased. Indeed the variations observed in region IV are generally

slower, indicating a reduced sticking coefficient and/or other slow processes. The II–IV break in the 173–193 K curves could have been taken to show an onset of islanding of an ordered phase. We can discount this possibility for two main reasons. First, no evidence of short-range ordering of superstructures has been seen in our diffraction maps between $T_x = 173$ –233 K and, in the higher coverage regions, only $p(1 \times 1)$ peaks are observed. Second, an anticipated intensity gradient break was not seen at the lower temperatures of 153 and 133 K, and at lower exposures.

Instead we propose that the end of region II corresponds to a marked decrease in sticking coefficient at the saturation of terrace sites with PH_3 (and/or PH_x and H fragments) and the slow intensity variations in region IV are associated with much slower adsorption process that can occur only in tandem with a finite molecular decomposition rate on terrace sites.

To support our above hypothesis, we must note the following observations:

1. The break from II to IV cannot correspond to a sticking coefficient drop to zero and the intensity variations being the result of decomposition alone; type IV intensity variations are not observed in the absence of PH_3 exposure.
2. The break from II to IV does not correspond to a jump in the sticking coefficient, caused by the sequential filling of different adsorption sites, in the absence of decomposition; short-range ordering is not observed as would be anticipated for sequential site filling.
3. We believe that the break from II to IV does not correspond to a jump in the sticking coefficient, such as may be anticipated for sequential filling of equivalent adsorption sites with but locally higher adsorbate–adsorbate coordinations, in the absence of decomposition; we have no viable reason for an apparent number density of the lower coverage sites that could decrease (by more than a factor of four) with increasing surface temperatures ($173 < T_x < 273$ K).
4. Decomposition most certainly occurs (to some degree) as the temperature is raised to as little as 250 K; H_2 desorption is seen at lower temperatures in the data of Fig. 3.

5. The magnitude of gradient in region IV increases, from 193 to 273 K, as the rate of thermally activated molecular decomposition must increase; this is consistent with an increased sticking coefficient associated with higher decomposition/fragmentation at higher surface temperatures.

Note, we are not suggesting that molecular decomposition stops once the PH_3 exposure is terminated. The absence of continued intensity decay, after completion of a PH_3 exposure, does not imply that decomposition has stopped. In decomposition the number density of molecular fragments must increase although, we propose, the specularly reflected He intensity may be largely unaffected. H appears “small” to the incident He atom! Adsorbed H can be significantly screened by the taller P containing fragments. Also, “H is small” implies that a PH_x fragment may appear to have an almost identical cross section to an adsorbed PH_3 molecule.

Molecular PH_3 decomposition may also be occurring earlier in regions I and II, for $T_x > 153$ K, although its effects can be masked by the other adsorption processes. We propose also that the ordering of region III may not be observed at 173 K, and above, in part due to the presence of molecular fragments, i.e. PH_x ($x = 1, 2$) or adsorbed H. The surface bound fragments in region IV must not be able to develop detectable short-range ordering.

At 193 K the initial defect sites require higher exposures to fill. Also a reduction in the initial sticking coefficient and/or initial cross section is evident in the smaller gradient of section II. In combination, we conclude that the sticking coefficient reduces as the surface temperature is raised above 153 K. N.B. Coadsorbates such as H, or PH_x fragments, are not anticipated to affect the *initial* (low coverage) sticking coefficients. Instead a surface temperature dependent initial sticking coefficient must be associated with at least partial energy accommodation before crossing a chemisorption barrier.

Region III as observed at low adsorption temperatures, $T_x < 153$ K, and the diffuse intensity maxima in Fig. 2, would imply the formation of a

poorly ordered $c(\sqrt{2} \times 3\sqrt{2})R45^\circ$ superstructure. This can be due to ordering of the molecular PH_3 species. In many other studies of molecular PX_3 adsorbate systems [16,17], the predominant binding configuration is taken to be the on-top site. Other sites are implied for PF_3 adsorption only at higher densities [25] (i.e. at the lowest adsorption temperatures). On the basis of the diffraction pattern we propose a structure of the $c(\sqrt{2} \times 3\sqrt{2})R45^\circ$ phase shown in Fig. 8, with a molecular density corresponding to $1/3$ ML. This structure, as shown, has one PH_3 molecule per primitive cell. Alternative higher density $c(\sqrt{2} \times 3\sqrt{2})R45^\circ$ structures, including more than one PH_3 molecule per primitive cell, can be discounted on the basis that they would require occupation of nearest neighbor sites. The Van der Waals radius of PH_3 normal to the C_3 axis can be estimated to be of order ~ 2.3 Å [26,27]. By comparison, nearest neighbor $\text{Cu}(001)$ sites are separated by only 2.55 Å, and next nearest neighbor sites by 3.61 Å. A simple Van der Waals interaction should not allow the high molecular density, as shown in Fig. 8. Yet, our quantitative

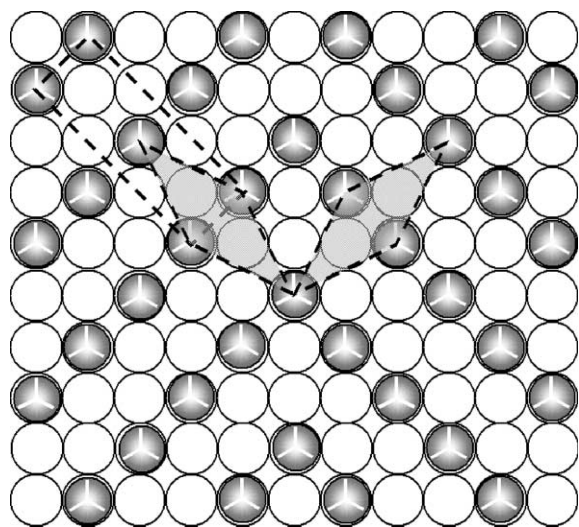


Fig. 8. A schematic representation of disordering (domain boundaries) in the low-temperature PH_3 saturated $c(\sqrt{2} \times 3\sqrt{2})R45^\circ/\text{Cu}(001)$ structure. A centered unit cell is marked by the dashed lines. Two (rotated) primitive unit cells are shown as shaded areas. Despite the patterned shading shown in the PH_3 species, we have no knowledge of the azimuthal orientations, nor their ordering (if any) of the adsorbed PH_3 molecules.

Auger intensity ratios are supportive of this same $1/3$ ML coverage for the low-temperature PH_3 saturation exposures. Both PF_3 and PH_3 exposed surfaces show indistinguishable P Auger line shapes. For the well ordered, $1/4$ ML, molecular PF_3 , $c(4 \times 2)$ structure $\text{AR}_{\text{PF}_3160} = 0.80$, and for the molecular PH_3 structure $\text{AR}_{\text{PH}_3140} = 1.02$. Their ratio, $\text{AR}_{\text{PH}_3}/\text{AR}_{\text{PF}_3} = 1.28$. From the Auger data alone we would predict $\Theta_{c(\sqrt{2} \times 3\sqrt{2})R45^\circ} = 1.28 \times 1/4 \text{ ML} \approx 0.32 \pm 0.02 \text{ ML}$. While the observed diffraction pattern is not well formed, and the structure cannot be well ordered, we still must take $1/3$ ML as our best estimate of the absolute P density in structures formed by PH_3 saturation at $T_x < 160$ K.

The observed hydrogen desorption between 250 and 320 K, shown in Fig. 3, clearly indicates at least partial PH_3 dissociation at these or lower surface temperatures. Certainly, for a $\text{Cu}(001)$ surface with adsorbed H only, H association and H_2 desorption reportedly takes place at $T_x = 270$ – 330 K [28,29]. In our studies of H desorption on otherwise clean $\text{Cu}(001)$, the helium reflectivity changes are strongest as T_x approaches 300 K. Also the facts, that the $c(6 \times 8)$ is formed either by PH_3 or by PF_3 exposure, and that identical Auger line shapes are observed, indicate that neither hydrogen nor fluorine is present within the $c(6 \times 8)$ phase. Namely, all the hydrogen is desorbed by 320 K.

The II–IV region breaks, indicating PH_3 saturation exposures, move to higher exposures as the adsorption temperature increases above 273 K. This can be explained by assuming that the saturated phosphine adsorption levels are limited by coadsorbed H and/or other molecular fragments. At $T_x > 273$ K the instantaneous H coverages decrease as T_x rises and PH_3 sticking does not saturate as early. This proposal is also supported by the fact that the higher P coverage $c(6 \times 6)$ phase can be produced only by exposures with T_x above 273 K.

Lastly, the phosphorus Auger line shape changes at $T_x = 240$ – 270 K, from the triplet to doublet form, suggesting an incorporation of all P atoms into at least the topmost plane of Cu (with a higher Cu coordination of P). We propose that the final increase in helium intensity, during the anneal

(Fig. 3) at 420 K, can be associated with an ordering and restructuring on the P incorporated surface. Indeed the best ordering in the $c(6 \times 8)$ phase is observed only after annealing to temperatures in excess of 420 K. The restructuring may involve lateral diffusion, and even diffusion of excessive P into the bulk. (The $c(6 \times 6)$ structure cannot be stabilized at $T_x > 473$ K.) The $c(6 \times 8)$ phase, once formed, is stable and can persist up to 900 K. The $c(6 \times 8)$ phase can be removed only by sputtering of the surface.

From the above information we propose the following sequence of events:

1. At $T_x < 160$ K molecular PH_3 adsorption occurs. At exposures >4 L a PH_3 structure with short-range ordering can be detected.
2. $160 \leq T_x \leq 193$ K adsorption of PH_3 or PH_x and H with a surface temperature dependent molecular sticking coefficient.
3. Onset of a decomposition/restructuring process at $T_x > 220$ K as indicated by a finite gradient in the region IV reflectivities.
4. Fast decomposition/restructuring process at $T_x = 240$ K marked by the maximum in helium reflectivity change (of Fig. 3).
5. Further decomposition at $T_x > 240$ K and H_2 desorption at $250 < T_x < 320$ K.
6. Incorporation of P atoms into the Cu plane, at $T_x \sim 240$ – 270 K, as indicated by the change in phosphorus Auger line shape.
7. At $T_x > 273$ K the $c(6 \times 8)$ phase can be formed.
8. At $T_x > 320$ K all H desorption finishes. PH_3 sticking is no longer hindered by adsorbed H levels. PH_3 saturation levels increase (with full PH_3 decomposition) and the surface can accommodate enough P for formation of the $c(6 \times 6)$ phase.
9. $T_x \sim 420$ K, onset of excessive P coverage depletion through diffusion into the Cu bulk. (The $c(6 \times 6)$ phase is lost, although the $c(6 \times 8)$ phase can persist.)

4.2. Structure of the surface phosphide phases

The observed $c(6 \times 6)$ and $c(6 \times 8)$ periodicities are unconventional. Only one fcc (001) metal

based $c(6 \times 6)$ phase has been reported; i.e. for submonolayer Ba films on Cu(001) [30]. However, absolute number densities of Ba are lower than presumed here for the P–Cu phase. (The size of a Ba atom is a much larger than for a P atom.) It is unlikely that these two structures would be inter-related.

The lack of fourfold symmetry displayed in the helium diffraction pattern from the $c(6 \times 6)$ structure automatically excludes all square plane groups (p4, p4mm, p4gm) as possible descriptors of the square superstructure. The remaining possible symmetry groups for this centered structure are the two rectangular plane groups (c2mm and cm) with a coincidence of lattice vectors, both equal to $6a_{\text{Cu}}$. Further analysis of the $c(6 \times 6)$ helium intensity patterns, such as displayed in Fig. 6(a), and their symmetries, indicates the necessity of unequal densities of four domains, each of the cm symmetry. Likewise, unequal densities of pairs of the four $c(6 \times 8)$ like domains is clearly seen in Fig. 6(b). We hence propose that the $c(6 \times 6)$ phase is closely related to a “compressed” version of the $c(6 \times 8)$ phase, obtained at lower P coverages. The one distinction between the two phases is that the $c(6 \times 6)$ structure is of the cm symmetry group, whereas the $c(6 \times 8)$ structure is that of the c2mm symmetry group. Our proposition entails a conservation of the number of phosphorus atoms per unit cell; a requirement being that there is exactly a 25% P coverage decrease in going from the $c(6 \times 6)$ to the ideal $c(6 \times 8)$ structure. (Incidentally the diffraction patterns from each $c(6 \times 6)$ domain also must have one mirror plane, but no inversion symmetry.)

The only information available to us regarding absolute P coverages comes from the Auger data. A minimum of a 20% increase in P sensitivity is seen after annealing of the molecular PH_3 to temperatures above ~ 273 K. The changes in P Auger line shape, associated with annealing, molecular decomposition, and phosphide formation, however, limit the applicability of published Auger sensitivity factors [31,32]. An alternative approach is to be used.

The complete $c(6 \times 6)$ structure gives the Auger P/Cu intensity ratio, $\text{AR}_{6 \times 6}$ of 1.72. The ideal $c(6 \times 8)$ structure should therefore display an in-

tensity ratio $AR_{6 \times 8} = 1.72 \times 36/48 = 1.29$. This is in excellent agreement with that obtained from an annealed, low-temperature-formed $c(\sqrt{2} \times 3\sqrt{2})$ - $R45^\circ$ phase, $AR_{PH36 \times 8} = 1.28 \pm 0.03$. Indeed the later phase appears very close to the ideal $c(6 \times 8)$ structure, in that (a) the $c(6 \times 8)$ and $c(6 \times 6)$ diffraction peaks are not coexisting (as they do at higher P coverages), and that (b) this structure displayed the maximum observed $(1/4, 0)/(0, 0)$ He diffraction peak intensity ratio. If the surface started at $1/3$ ML, if phosphines do not desorb during the anneal process (not observed), and if P interdiffusion rate is low at the anneal temperature (523 K), the ideal $c(6 \times 8)$ phase must have a coverage $\Theta_{6 \times 8} \lesssim 1/3$ ML. The upper limit of $1/3$ ML corresponds to a phosphorus density of 16 P/centered unit cell (i.e. 8 P/primitive unit cell) and a coverage of $\Theta_{6 \times 6} = 0.44$ ML for the $c(6 \times 6)$ phase.

Lastly, a large fraction of the backscattered helium intensity lies within the narrow rainbow angle of $4 \pm 1^\circ$. Alone, this would be indicative of a low corrugation on the surface. However, the presence of a wider rainbow angle may imply that at least some (but not all) of the surface (unit cell) displays a shorter wavelength and/or deeper corrugation.

Given the above information regarding the $c(6 \times 6)$ and $c(6 \times 8)$ phases, below we argue the “pros and cons” for various approaches to construction of models for the observed structures. Any structural model for the $c(6 \times 6)$ phase must show a “high” P coverage. By way of elimination, a simple substitutional $(\sqrt{2} \times \sqrt{2})R45^\circ$ phase would show a coverage as high as 0.5 ML. But is not apparent, to these authors, how such a structure could be modified to produce the required registry of the $c(6 \times 6)$ phase as well as to remove the fourfold symmetry.

There exist two well-documented bulk copper phosphide phases: “copper-rich” Cu_3P [22] and “phosphorous-rich” CuP_2 [21]. The structure with proportionately less Cu, CuP_2 , is monoclinic with the P atoms forming corrugated layers parallel to the (100) plane, each layer being a continuous sheet built from ten-membered P atom rings. But, the Cu_3P phase may be more pertinent to our surface reconstruction, as it is formed above an

excess of Cu substrate atoms. Cu_3P has a hexagonal unit cell ($a = 6.9593 \text{ \AA}$, $c = 7.143 \text{ \AA}$), in essence constructed of four alternating rumpled layers: Cu_2 , CuP , Cu_2 , CuP . A schematic of a Cu – P layer is depicted in Fig. 9. Note, the rumpling implies Cu atoms are either above or below the plane of P atoms. The neighboring copper layers, above and below a Cu – P layer, are also very rumpled and are placed in such a way that one of the Cu atoms of each of these layers are directly above or below a P atom. Each P has essentially 11 (non-equivalent) nearest Cu neighbors with a Cu – P separation of approximately 2.35 – 2.37 \AA [22] in the bulk Cu_3P phase.

The open Cu – P rings of the Cu_3P structure have a planar P density of $1 \text{ P}/(14.0 \text{ \AA}^2)$. For comparison, the suggested P density of the $c(6 \times 6)$ phase, with $\Theta_{6 \times 6} = 0.44$ ML, is $1 \text{ P}/(14.8 \text{ \AA}^2)$. A small compression of the open hexagonal Cu – P ring structure would give the correct density, but not the correct unit cell shape and symmetry. (Even with an 9.9% expansion along one axis of the ring structure, and an 5.0% compression along a perpendicular direction, only a $p(3 \times 3)$ phase is obtained and not the desired $c(6 \times 6)$ phase.)

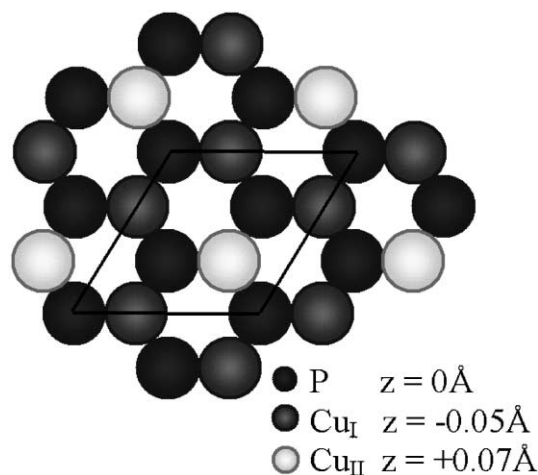


Fig. 9. Schematic of a phosphorus and copper containing layer in the bulk Cu_3P crystal structure. Phosphorus atoms are shaded in black, and copper atoms are designated by the grayed circles. Note: two non-equivalent copper atoms exist, which are either raised or lowered with respect to the plane of phosphorus atoms.

Although the open ring hexagonal structure appears not to have all the features required for formation of the $c(6 \times 6)$ phase, it does have one redeeming quality, in that the superposition of any hexagonal structure on top of the fourfold substrate will remove one mirror plane symmetry of the overall unit cell, and cm symmetry remains.

A number of fcc (001) metal surfaces have displayed hexagonal reconstructions of the top-most surface layer, namely Ir(001) [33], Pt(001) [34] and Au(001) [35–37]. Ab initio studies [38] have suggested that this type of reconstruction is favored for the 5d series only, and is not anticipated (nor observed) for the pure copper surface. However a similar type of hexagonal reconstruction has been observed for Cu_2Si overlayers produced by adsorption of Si on Cu(001) [39,40] through SiH_4 exposure. In the Cu_2Si stoichiometry surface, high-order periodicities originate from the discommensurations of the topmost layer with the substrate structure.

A mixed stoichiometry, hexagonal overlayer, type of reconstruction has a basically close packed surface layer that, to an incoming helium atom, may also exhibit a comparatively small corrugation. (The P could be incorporated within the surface plane. This should be compared to a case with a more open structure including phosphorus atoms in the topmost plane, that would show much more intense, wide angle diffraction peaks.)

Based on the arguments above, we propose a model which is schematically presented in Fig. 10. The dimension of the reconstructed primitive unit cells are shown by the solid line. Both $c(6 \times 6)$ and $c(6 \times 8)$ phases are essentially identical in that they have uniaxially stretched or compressed hexagonal Cu_2P overlayers.

The $c(6 \times 6)$ phase has a surface layer that is under a 15.5% compression from the hexagonal mesh of 2.55 Å lattice parameter (i.e. that for the pure Cu(001) surface density). In contrast, the $c(6 \times 8)$ phase has a surface layer that is under a 15.5% expansion. Our justification for leaving a “hole” in the mesh is to introduce a means for stress relief. In the models of Fig. 10, no attempt has been made to show the relaxations that must occur in these structures. The only conceptual difference in the two structures is the size of the

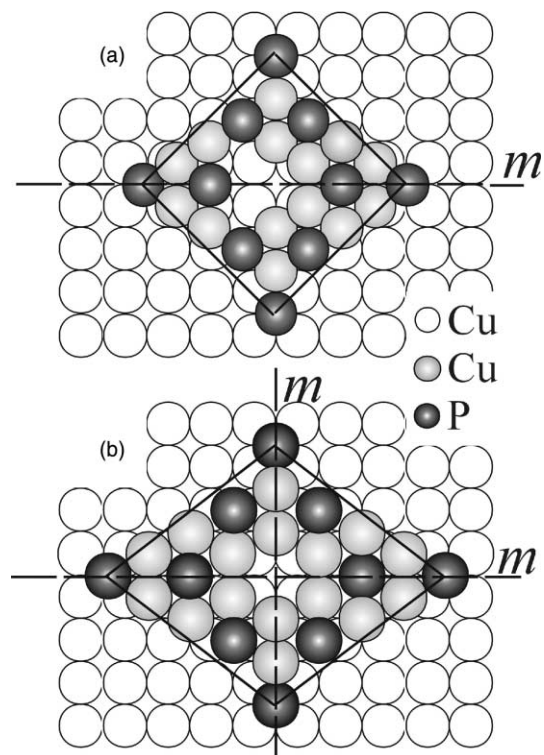


Fig. 10. Schematic diagrams showing proposed models for the surface layer phosphorus and copper atoms on Cu(001) in the (a) $c(6 \times 6)$ and (b) $c(6 \times 8)$ structures. Subsurface copper atoms, of the non-reconstructed substrate, are drawn in white. Top layer (shaded) atoms show copper in light gray and phosphorus atoms (darker shading), with an overall 2-D stoichiometry close to Cu_2P .

hole. Higher stresses in the most compressed phase, may require the removal of two copper atoms as well as a P atom from the surface layer. In contrast, the lower surface density phase may require only the removal of one (P) atom. This speculation is introduced essentially because of the different observed symmetries. The removal of one (P) atom alone maintains a $c2mm$ symmetry of the overall $c(6 \times 8)$ structure. Whereas, a cm symmetry of the $c(6 \times 6)$ structure is established through the removal of three atoms (two Cu and P).

Other complexities may be introduced into other proposed structures. Such complexities may include the addition of another layer, or multilayer structures, in the unit cells, e.g. Cu(111)-like lay-

ers above or below the Cu_2P layer. We are not able to discount such ideas, however, supporting evidence is not available.

Lastly we should mention that our efforts to construct more simple rectangular unit cells have failed. All our attempts along these lines either, do not produce a centered unit cell, or do not give rise to sufficiently high P densities, or have required too high a P atom density.

Clearly our suggested models above are not unique, but they would show the essential features of the data available to us. The majority of the surface areas are densely packed and should show the observed low He rainbow angles. The hole in the structure can introduce a wider rainbow angle. The symmetries of the diffraction patterns would be reproduced. A strictly non-planar structure, as proposed, would remove an inversion symmetry from the $c(6 \times 6)$ phase diffraction pattern, as additional phase shifts are associated with height variations across the unit cell. Unfortunately, the drift spectra could not be used to show two clear height levels within the unit cell. For both our models, the P atom densities are as high as 7 P/primitive unit cell.

5. Summary

We have presented results of helium scattering studies of phosphine adsorption on the $\text{Cu}(001)$ surface and of copper–phosphorus phase formation. Below 160 K PH_3 adsorbs molecularly, at $160 < T_x < 273$ K molecular fragments PH_x can predominate, while above 273 K phosphorus is deposited. The diffraction pattern from the low-temperature saturated surface exhibited short-range order in a “ $c(\sqrt{2} \times 3\sqrt{2})R45^\circ$ phase” with $1/3$ ML phosphorus coverage. Phosphine does not desorb molecularly. Instead a molecular decomposition occurs which can be initiated at temperatures as low as 150 K. We have suggested that the He atom reflectivity is not sensitive to the thermally induced decay process directly, but is instead sensitive to a slower adsorption rate that tracks the slow decomposition processes. PH_3 uptake is also affected by the extent of decomposition and adsorbed H levels.

Either by annealing of a low temperature exposed phosphine phase, or by phosphine deposition at room temperature or above, well-ordered copper–phosphorus structures are produced which exhibit $c(6 \times 8)$ or $c(6 \times 6)$ diffraction patterns. Possible models for these structures have been proposed that are based on the formation of a quasi-hexagonal Cu_2P overlayer over the square copper substrate lattice.

Acknowledgements

This work was supported by NSF-CHE 9820061. L.V.G. would also like to thank G. Popov for assistance with the software and D.V. Potapenko for many helpful discussions.

References

- [1] Y. Ohshita, H. Kitajima, *J. Appl. Phys.* 70 (1991) 1871.
- [2] S. Kobayashi, M. Iizuka, T. Aoki, N. Mikoshiba, M. Sakuraba, T. Matsuura, J. Murota, *J. Appl. Phys.* 86 (1999) 5480.
- [3] X. Huang, T. Taishi, I. Yonenaga, K. Hoshikawa, *Jpn. J. Appl. Phys.* 40 (2001) 12.
- [4] B.S. Meyerson, W. Olbricht, *J. Electrochem. Soc.* 131 (1984) 2361.
- [5] B.S. Meyerson, M.L. Yu, *J. Electrochem. Soc.* 131 (1984) 2366.
- [6] L. Kipp, R.D. Bringans, D.K. Biegelsen, J.E. Northrup, A. Garcia, L.-E. Swartz, *Phys. Rev. B* 52 (1995) 5843.
- [7] C.A. Tolman, *Chem. Rev.* 77 (1977) 313.
- [8] H.-S. Tao, Ph.D. Thesis, Rutgers University, New Brunswick, New Jersey, 1994.
- [9] H.-S. Tao, U. Diebold, N.D. Shinn, T.E. Madey, *Surf. Sci.* 375 (1997) 257.
- [10] X.-L. Zhou, J.M. White, *Surf. Sci.* 221 (1989) 534.
- [11] M.D. Alvey, J.T. Yates Jr., *J. Chem. Phys.* 87 (1987) 7221.
- [12] R.I. Hedge, J.M. White, *J. Phys. Chem.* 90 (1986) 2159.
- [13] G.E. Mitchell, M.A. Henderson, J.M. White, *Surf. Sci.* 191 (1987) 425.
- [14] R.I. Hedge, J.M. White, *Surf. Sci.* 157 (1985) 17.
- [15] M. Kiskinova, D.W. Goodman, *Surf. Sci.* 108 (1981) 64.
- [16] R.G. Jones, N.E. Abrams, G.J. Jackson, N.A. Booth, M.T. Butterfield, B.C.C. Cowie, D.P. Woodruff, M.D. Crapper, *Surf. Sci.* 414 (1998) 396.
- [17] G.J. Jackson, J. Ludecke, D.P. Woodruff, A.S.Y. Chan, N.K. Singh, J. McCombie, R.G. Jones, B.C.C. Cowie, V. Formoso, *Surf. Sci.* 441 (1999) 515.

- [18] L.V. Goncharova, J. Braun, A.V. Ermakov, G.G. Bishop, D.-M. Smilgies, B.J. Hinch, *J. Chem. Phys.* 115 (2001) 7713.
- [19] C.T. Rettner, H.A. Michelsen, D.J. Auerbach, C.B. Mullins, *J. Chem. Phys.* 94 (1991) 7499.
- [20] B. Poelsema, G. Comsa, *Scattering of Thermal Energy Atoms from Disordered Surfaces*, Springer-Verlag, Berlin, 1989.
- [21] O. Olofsson, *Acta Chem. Scand.* 19 (1965) 229.
- [22] O. Olofsson, *Acta Chem. Scand.* 26 (1972) 2777.
- [23] M. Sancrotti, F. Ciccacci, M. Fanfoni, P. Chiaradia, *Phys. Rev. B* 42 (1990) 3745.
- [24] M. Sancrotti, F. Ciccacci, M. Fanfoni, P. Nataletti, P. Chiaradia, *Surf. Sci.* 211–212 (1989) 651.
- [25] J. Braun, G.G. Bishop, A.V. Ermakov, L.V. Goncharova, B.J. Hinch, *J. Chem. Phys.* 110 (1999) 5337.
- [26] D.R. Lide (Ed.), *CRC Handbook of Chemistry and Physics*, 74th ed., CRC Press, Boca Raton, 1993.
- [27] D.E.C. Corbridge, *The Structural Chemistry of Phosphorus*, Elsevier, Amsterdam, 1974.
- [28] I. Chorkendorff, P.B. Rasmussen, *Surf. Sci.* 248 (1991) 35.
- [29] G. Anger, A. Winkler, K.D. Rendulic, *Surf. Sci.* 220 (1989) 1.
- [30] S. Bartholmei, P. Fouquet, G. Witte, *Surf. Sci.* 473 (2001) 227.
- [31] L.I. Davis, N.C. McDonald, P.W. Palmberg, *Handbook of Auger Electron Spectroscopy*, Physical Electronics Inc., Minnesota, 1976.
- [32] D. Briggs, M.P. Seah, *Practical Surface Analysis*, second ed., Wiley, New York, 1990.
- [33] N. Bickel, K. Heinz, *Surf. Sci.* 163 (1985) 435.
- [34] K. Kuhnke, K. Kern, G. Comsa, W. Moritz, *Phys. Rev. B* 45 (1992) 14388.
- [35] D. Gibbs, B.M. Ocko, D.M. Zehner, S.G.J. Mochrie, *Phys. Rev. B* 42 (1990) 7330.
- [36] S.G.J. Mochrie, D.M. Zehner, B.M. Ocko, D. Gibbs, *Phys. Rev. Lett.* 64 (1990) 2925.
- [37] D.L. Abernathy, S.G.J. Mochrie, D.M. Zehner, G. Grubel, D. Gibbs, *Phys. Rev. B* 45 (1992) 9272.
- [38] V. Fiorentini, M. Methfessel, M. Scheffler, *Phys. Rev. Lett.* 71 (1993) 1051.
- [39] A.P. Graham, B.J. Hinch, G.P. Kochanski, E.M. McCash, W. Allison, *Phys. Rev. B* 50 (1994) 15304.
- [40] G.G. Bishop, A.P. Graham, K. Mihanic, J.K. Wendel, B.J. Hinch, G.P. Kochanski, *Phys. Rev. Lett.* 79 (1997) 1409.